Phenomenological universalities: a novel tool for the analysis of dynamic contrast enhancement in magnetic resonance imaging

2011 Phys. Med. Biol. 56 573

(http://iopscience.iop.org/0031-9155/56/3/004)

IOP PUBLISHING PHYSICS IN MEDICINE AND BIOLOGY

Phys. Med. Biol. **56** (2011) 573–586 doi:10.1088/0031-9155/56/3/004

Phenomenological universalities: a novel tool for the analysis of dynamic contrast enhancement in magnetic resonance imaging

A S Gliozzi[1], S Mazzetti[1,2], P P Delsanto[1], D Regge[2] and M Stasi[2]

[1] Physics Department, Politecnico di Torino, 10129 Torino, Italy
[2] IRCC, Institute for Cancer Research and Treatment, Candiolo, Torino, Italy

E-mail: antonio.gliozzi@polito.it, simone.mazzetti@polito.it, pier.delsanto@polito.it, daniele.regge@ircc.it and mstasi@mauriziano.it

Received 20 June 2010, in final form 27 October 2010
Published 6 January 2011
Online at stacks.iop.org/PMB/56/573

Abstract

Dynamic contrast enhancement in magnetic resonance imaging (DCE-MRI) is a promising tool for the clinical diagnosis of tumors, whose implementation may be improved through the use of suitable hemodynamic models. If one prefers to avoid assumptions about the tumor physiology, empirical fitting functions may be adopted. For this purpose, in this paper we discuss the exploitation of a recently proposed phenomenological universalities (PUN) formalism. In fact, we show that a novel PUN class may be used to describe the time–signal intensity curves in both healthy and tumoral tissues, discriminating between the two cases and thus potentially providing a convenient diagnostic tool. The proposed approach is applied to analysis of the DCE-MRI data relative to a study group composed of ten patients with spine tumors.

Introduction

Magnetic resonance imaging (MRI) is a versatile imaging modality and an indispensable tool in modern diagnostic medicine, with a wide range of applications (Tsekos *et al* 2008). The most frequently used MRI method in medicine is the anatomical MRI designed to differentiate tissue structures (Fayed *et al* 2006). MRI can produce high-resolution images in multiple different planes of the interior of the body non-invasively and without the hazard of ionizing radiation (Yankeelov and Gore 2009).

The intrinsic contrast between soft tissues and many pathological ones is sufficiently great, so that often contrast agents (CAs) are not needed. Nonetheless, appropriate exogenous CAs have been developed for use with MRI and are safely employed in many clinical imaging procedures (van Cara *et al* 1999). MRI CAs are pharmaceuticals, administered to a subject

during the imaging procedure, that are designed to increase the contrast between different tissues. CAs alter the MRI signals and, when they are introduced into the body, they decrease the relaxation times of the tissue water with which they come into contact, in a way which depends on how the CAs are distributed within the tissue (Yankeelov and Gore 2009). For a given region of interest (ROI) the temporal characteristics of the signal intensity (SI) as the CAs pass through the tissue can be studied and useful information on its physiology and pathology can be derived (Verstraete and Lang 2000).

In a typical dynamic contrast enhancement (DCE) MRI imaging session, a ROI is selected for study (e.g. a suspected region) and MR images are collected before, during, and after a CA is injected into a vein of a patient. Each image acquired corresponds to one time point, and each pixel in each image can be extracted to find out its own time course, which can then be analyzed with a mathematical model. There are different methods to analyze these dynamic data and, among them, semiquantitative parameters may be employed in most routine settings without the need of specialized software (Tuncbilek *et al* 2005). These parameters are proved to be indirect determinants of tumor microcirculation and tissue perfusion (Buadu *et al* 1996, Tuncbilek *et al* 2004, 2003).

Materials and methods

The study group comprised ten patients with spine tumors (whose morphology and histology make our analysis especially meaningful, since they were all bone metastases from breast cancer). All of them underwent MR imaging with a 1.5 T whole body scanner (Signa HDx, GE, Milwaukee) and an eight-channel cervical-thoracic-lumbar (CTL) receiver coil. Conventional MRI series (sagittal T1, T2 and Short TI inversion recovery (STIR)) were used to locate tumoral lesions and exhibit their morphologic characteristics. After these preliminary series, four precontrast sagittal 3D SPoiled GRadient echo (SPGR) sequences (TR/TE/NEX/FA: 6.8ms/2 ms/1/24°, band width: 25 kHz, slice thickness: 4 mm, matrix: 256 × 192 are used to minimize artifacts (Taber *et al* 1998, Claude *et al* 2000)) were acquired as baseline images (see figure 1 as an example of slice location). After the precontrast sequences, patients were given 0.1 mmol kg^{-1} gadobutrol (Gadovist, Bayer Schering, Berlin, Germany) intravenously through a peripheral line at 0.7 ml s^{-1}, using a power injector (Medrad Spectris, Maastricht, The Netherlands), followed by an infusion of 20 cc normal saline at the same velocity. In the contrast sequence, a multiphase sagittal 3D SPGR was applied with parameters identical to those used for the precontrast sequence. For each patient a total of 31 phases were acquired sequentially, each lasting 16 s, for a total time of 8 min.

At the end of the exam, all the images acquired before (baseline), during and after CA injection were transferred from the scanner to a workstation for data analysis. For each patient a ROI was manually selected including the lesion (the most enhanced region); see figure 2. When a tumor was extended in more than a single slice, the ROI was drawn including multiple images. The malignant ROIs covered areas between 0.15 and 1.5 cm^2. The SI of a lesion was computed as the mean gray value of the pixels belonging to the same ROI. For each patient, the baseline point was obtained as the mean of the four SIs in the precontrast acquisitions. A non-enhancing region containing the same type of tissue as in the tumor ROI was also selected for each patient, with an extension approximately equal to the tumoral one, in order to make a comparison between the behavior of the two different DCE curves in both malignant and non-tumoral bones (in the following we will call the latter a 'normal tissue region'). Each dataset was normalized by subtracting to each time point the mean precontrast value computed on the selected ROI. Then the signal intensities were plotted versus time for each patient.

Figure 1. Images showing an example of slice location in the three plane views for DCE sequence acquisition in the sagittal direction.

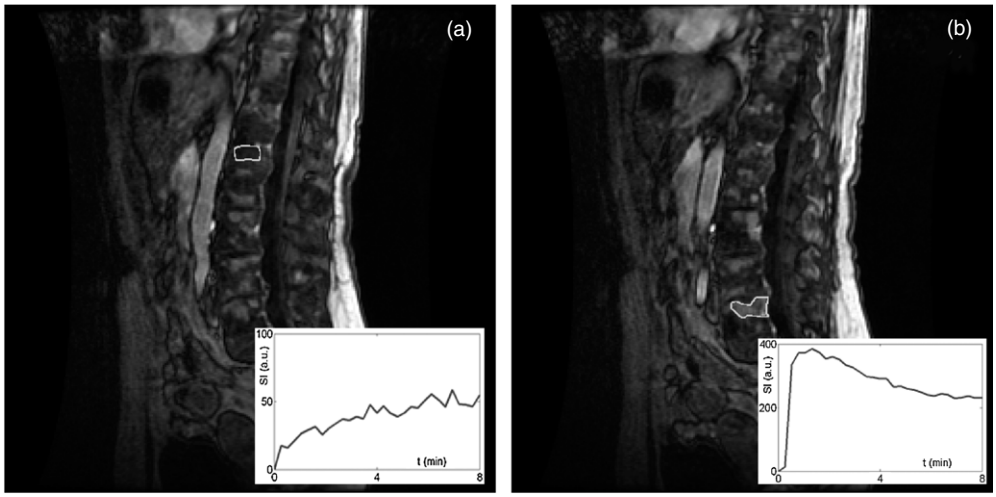

Figure 2. Examples of typical ROI localization drawn on DCE sagittal images and corresponding dynamic contrast enhancement curves for both normal tissue (a), and a tumoral lesion (b). Note the different scales for the SI axes in the two cases.

Evaluation of kinetic variables from DCE-MRI

There are two physiological processes that accompany the faster growth rate of many tumors: an increased number of vessels and, along with it, an increased permeability. Therefore one can expect an augmented overall signal enhancement in the proximity of tumors (due to a greater vascular volume), a larger vessel permeability, and increased flow (Srikanchana *et al* 2004, Knopp *et al* 2001, Scalerandi and Sansone 2002).

Extraction of hemodynamic parameters from DCE-MRI data requires the calculation of contrast medium concentration as a function of time, $C(t)$, either in each image voxel or in the ROI (Fan *et al* 2007). Several pharmacokinetic and empirical models for DCE-MRI hemodynamic parameter estimation have been developed (Gal *et al* 2007a, Wilburn *et al* 1999, Rijpkema *et al* 2001, Montemurro *et al* 2004). In the simplest model of tissue signal

enhancement one considers three parameters: maximum signal enhancement, the rate of initial enhancement ('wash-in'), and the rate of increased signal decay ('wash-out').

Quantitative techniques that are often combined with rapid temporal sampling have been employed together with pharmacokinetic models of tissues, to evaluate the parameters. These models require assumptions about the CA perfusion process and the water exchange rates between prescribed tissue compartments. Among them one finds the general kinetic models (Daldrup *et al* 1998), the Tofts (Tofts and Kermode 1991, Tofts *et al* 1999) and Brix models (Brix *et al* 1991), which allow us to evaluate a variety of parameters, depending on the model.

For the implementation of these kinds of analyses, some prior knowledge is typically required in order to fit the measured DCE-MRI data. This prior knowledge is usually introduced as additional parameters (e.g. model of bolus injection (Hayton *et al* 1996), tissue relaxivity (Rijpkema *et al* 2001)) to be estimated for each study, or statistically inferred from previous works (Tofts *et al* 1995, Furman-Haran and Degani 2002). However, the significance of such parameters' evaluation depends on the validity of the theoretical model and on the assumptions used to interpret the data. This fact can add noise and/or bias to the model-fitting process, thus reducing the validity of the procedure. Computed quantities are highly dependent on the method of analysis; thus, a comparison of results from different models is difficult (Srikanchana *et al* 2004).

Furthermore, pharmacokinetic models do not always provide a good fit to experimental data, and therefore they have a limited diagnostic utility (Fan *et al* 2007). Consequently, three or more compartment models were formulated in order to obtain a more realistic hemodynamic description (Port *et al* 1999), each time with increasing complexity. Also, physiological models require a knowledge of the contrast medium concentration in the blood as a function of time (arterial input function (AIF)). Sometimes measuring the AIF is very difficult, causing errors in the determination of tracer kinetics.

To overcome the problems associated with limited SNR, semiquantitative analysis of DCE-MRI data can be performed. In this kind of analysis $C(t)$ is not fitted, but contrast medium uptake and washout are analyzed by simply classifying contrast medium kinetics. Some common diagnostic parameters include the initial area under the curve, signal enhancement ratio, maximum slope, time to peak of enhancement, washout ratio and so on (Pickles *et al* 2009).

One of the most commonly used approaches in clinical evaluation has been proposed by Kuhl *et al* (1999) and consists of a classification of curves according to the intermediate and late postcontrast phases (either wash-out, plateau or persistent behavior). This simplified approach allows one to analyze only a limited part of the acquired curve (e.g. a single point, if the maximum or time to maximum enhancement is studied, or a few points if slopes are computed), thus yielding a local description of the curve, rather than a global view.

As an alternative to these approaches, empirical functions can be used to fit $C(t)$ accurately, without the need of assumptions about tumor physiology. Unfortunately, however the mathematical functions employed so far do not have the flexibility to accurately describe contrast uptake and wash-out for long periods of time (Fan *et al* 2007). Among them we recall the Weibull function (Gal *et al* 2007b)

$$y_{\mathrm{weib}}(t) = At\exp(-t^B) \tag{1}$$

with only two fitting parameters (A and B) and the biexponential function

$$y_{\mathrm{biexp}}(t) = a\exp(bt) + c\exp(\mathrm{d}t), \tag{2}$$

where the coefficients b and d (both negative) represent the rapidity of the wash-in and wash-out phases and the parameters a and c their weights.

Phenomenological universalities as a tool for dataset analysis

The fitting of any given set of experimental data may be just an exercise to find, for practical purposes, a convenient analytical curve to represent the data or, at a much deeper level, it may aim to provide a model. In the latter case one should restrict one' s attention to the raw data and analyze them independently of the field of application. Such an unbiased procedure may be provided by the phenomenological universalities (PUN) approach, recently proposed by Delsanto and collaborators (Castorina *et al* 2006, Delsanto 2007) and applied to a wide range of applications (auxology (Delsanto *et al* 2008), tumor growth (Gliozzi *et al* 2010, 2009), nonlinear elasticity (Delsanto *et al* 2009), and others (Pugno *et al* 2008, Barberis *et al* 2010)).

In order to describe PUN methodology from an applicative point of view, let us start with the first-order nonlinear growth differential equation

$$\frac{\mathrm{d}y}{\mathrm{d}t} = a(y)y, \tag{3}$$

where $a(y)$ represents the (unknown) growth rate. Equivalently, equation (3) may be written as

$$\frac{\mathrm{d}z}{\mathrm{d}t} = a(z), \tag{4}$$

where $z = \ln(y)$. To integrate equations (3), or (4), it is necessary to make some assumption on the rate a, as suggested, e.g., from an analogy of equation (4) with the equations of motion in dynamics. In them z represents the displacement, $a = \frac{\mathrm{d}z}{\mathrm{d}t}$ the velocity and $b = \frac{\mathrm{d}a}{\mathrm{d}t}$ the acceleration. Assuming a viscous medium, the force (and therefore b) is proportional, in a first approximation, to the velocity. We can correspondingly assume that b is given by an expansion in $\frac{\mathrm{d}z}{\mathrm{d}t}$, i.e.

$$b = \sum_{i=1}^{N} c_i a^i(t) = \beta a + \gamma a^2 + \cdots. \tag{5}$$

For example, for $N = 2$ we have, in addition to the linear term βa, also the quadratic term γa^2.

We call UN the class generated by the solution of the coupled differential equations (4) or (3) and (5), when in the latter only the first N terms are considered. The functions $y(t)$ that one obtains for the first UN classes ($N = 0, 1, 2$) have a very wide range of applications. In fact

- for $N = 0$, i.e. U0, $b = 0$; $y(t)$ represents a self-catalytic growth function. By integrating over the two ODE's, equations (5) and (3), we obtain

  $$y(t) = \exp(a_0 t), \tag{6}$$

  where $a_0 = a(t = 0)$. Here and in the following we normalize the variable $y(t)$, so that $y(0) = 1$.
- for $N = 1$, i.e. U1, $b = \beta a$ and

  $$y(t) = \exp[a_0/\beta(\exp(\beta t) - 1)]. \tag{7}$$

  Equation (7) yields the Gompertz law (Gompertz 1825), which has been extensively used in all kinds of growth problems for almost two centuries.
- for $N = 2$, i.e. U2, $b = \beta a + \gamma a^2$ and

  $$y(t) = \exp[1 + a_0\gamma/\beta(1 - \exp(\beta t))]^{-1/\gamma}, \tag{8}$$

  which represents a generalization of West's law (West *et al* 2001, West and Brown 2004, West *et al* 2000).

In the absence of further information, one can obviously consider any other kind of assumptions for the relationship $b(a)$ of equation (5) and, correspondingly, obtain novel PUN classes, different from UN. For example, it is tempting (for completeness) to include in equation (5) a constant term α. We call the thereby generated classes EUN (i.e. extended UN), e.g.

- for $N = 0$, i.e. EU0, $b = \alpha$ and

$$y(t) = \exp\left(a_0 t + \tfrac{1}{2}\alpha t^2\right). \tag{9}$$

- for $N = 1$, i.e. EU1, $b = \alpha + \beta a$ and

$$y(t) = \exp\left[rt + \frac{1}{\beta}\left(a_0 - r\right)\left(\exp(\beta t) - 1\right)\right], \tag{10}$$

where $r = \frac{\alpha}{\beta}$.

Formally EUN corresponds, for the kind of integrations performed, to U(N+1). Therefore we are not considering here further EUN classes beyond EU1.

Application of the EUN formalism to DCE-MRI

A remarkable result of our study is that the class EU1 (which had never been considered before) may be advantageously employed for the evaluation of DCE-MRI functional studies. In them, several variables are estimated (Verstraete *et al* 1994, van der Woude *et al* 1998), e.g. start of tumor enhancement (time interval between start of arterial and tumor enhancement), spatial pattern and progression. The latter has been utilized for the classification in five different types of the time–SI curves (van Rijswijk *et al* 2004). Figure 3 shows that all five types may be obtained in the framework of EU1 (no example of type I is included, since it corresponds to a flat curve with no enhancement). It is important to remark that while healthy tissues may yield curves belonging to any of the five types, only curves of the type IV correspond to tumoral tissues.

As it can be seen from equation (10), the EU1 function has three parameters a_0, β and r, upon which all the features of the SI curves depend.

- a_0 controls the steepness of the curve at $t = 0$. Together with β it primarily affects the growth rate of the curve in its first part.
- β is in inverse proportion to the time the system takes to reach the knee of the curve.
- The sign of $r = \frac{\alpha}{\beta}$ determines the behavior of the second part of the curve and its absolute value is linked to the rapidity of the change. For $r > 0$, one can observe a further enhancement of the intensity of the signal, while for $r < 0$ there is a wash-out phase.

For some particular values of the parameters, it is possible to predict other features of the curves. For example, in the case when $\alpha = 0$ (types II and III), it is easy to calculate the value of the plateau:

$$y_{\mathrm{pl}} = \exp\left(-\frac{a_0}{\beta}\right). \tag{11}$$

In this case the parameter $1/\beta$ can be viewed as a 'characteristic time' of the system, i.e. the time needed to reach $1 - 1/\mathrm{e}^e$ (i.e. 93%) of the asymptotic value y_{pl}.

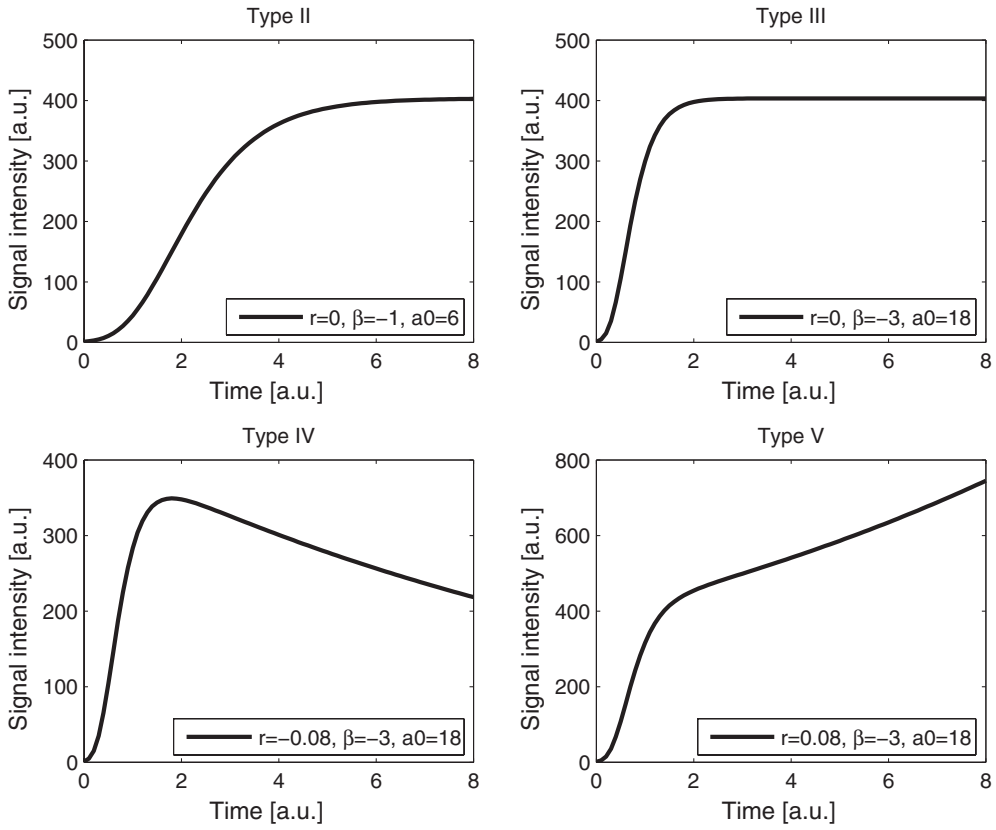

Figure 3. Classification of time–SI curves (van Rijswijk *et al* 2004): type II, gradual increase of enhancement; type III, rapid initial enhancement followed by a plateau; type IV, rapid initial enhancement followed by a washout phase; and type V, rapid initial enhancement followed by sustained later enhancement. Type I is a flat curve with no enhancement and therefore is not reported in the figure for brevity.

Results

For each of the ten patients with spine tumors involved in our study, DCE-MRI SI curves were analyzed for both a healthy and a tumoral body region. The resulting 20 curves were fitted by means of the EU1 function, equation (10). For a comparison, two fitting functions, i.e. the Weibull function, equation (1), and the biexponential function, equation (2), were also considered. In order to evaluate the quality of the results, the standard R^2 criterion was employed.

The results of the fitting with EU1 are very promising (particularly for tumoral tissues). For brevity only the curves corresponding to four out of the twenty cases in the study are shown in figure 4. Their respective R^2 values are reported in table 1. It is clear from the table that the EU1 results are generally much better than the ones obtained with the biexponential function, even if the former has only three parameters versus four of the latter. They are even better than those obtained with the Weibull function, which, however, has only two parameters. Similar results are obtained in the other 16 cases; they are not reported in figure 4, for brevity, but the mean values of R^2 are considerably better for EU1 than for the other two functions

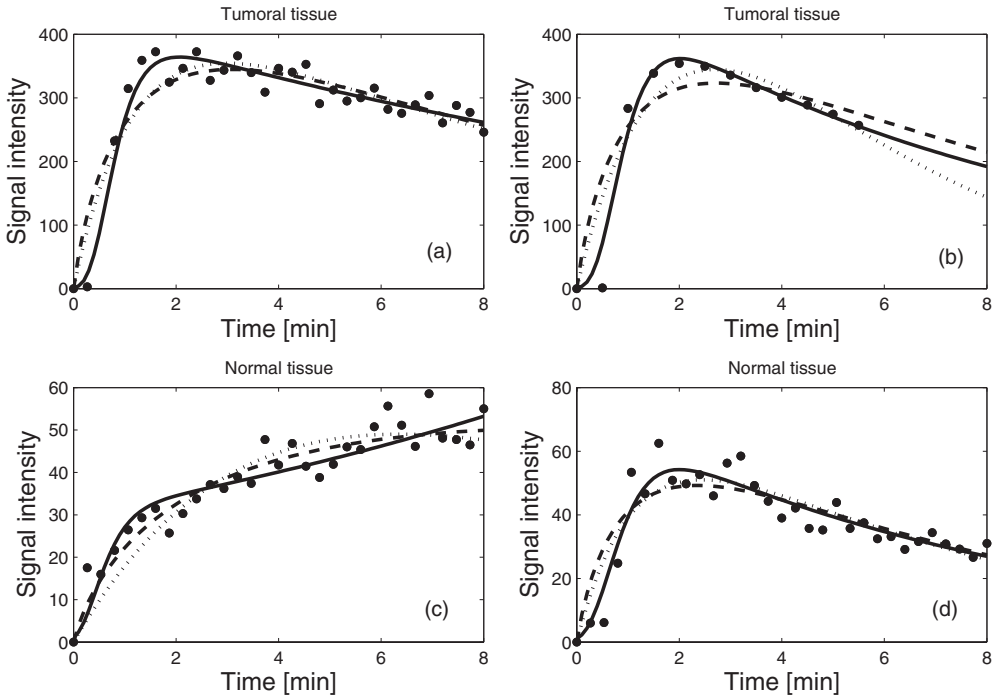

Figure 4. Fitting of the DCE curves for the three fitting functions considered: EU1 (continuous lines), biexponential (dotted lines) and Weibull (dashed lines). Curves for four different cases are shown, two for tumoral tissues (plots a and b) and two for healthy tissues (plots c and d). The corresponding R^2 values are reported in table 1.

Table 1. Values of R^2 for the three fitting functions used in figure 4, and the mean values (and corresponding standard deviation) of R^2 for all the ten patients considered (both normal and tumoral tissues).

Plots	EU1	Biexponential	Weibull
a	0.92	0.84	0.78
b	0.96	0.86	0.78
c	0.86	0.88	0.89
d	0.88	0.79	0.74
Mean value norm. tiss.	0.79 ± 0.12	0.67 ± 0.20	0.67 ± 0.21
Mean value tumoral tiss.	0.86 ± 0.07	0.75 ± 0.09	0.71 ± 0.09

(biexponential and Weibull) for both normal and tumoral tissues (see the last two lines of table 1).

We have also calculated for the 20 cases considered the mean values and standard deviations of the EU1 parameters (r, β and a_0), distinguishing between healthy and tumoral tissues. They are reported, together with the values M of the SI maxima, in table 2. It is remarkable that no real difference between healthy and tumoral tissues can be observed for the parameters r and β (except for a much larger standard deviation in the former, particularly for r). Conversely, there is a very clear separation between the two cases (healthy and tumoral

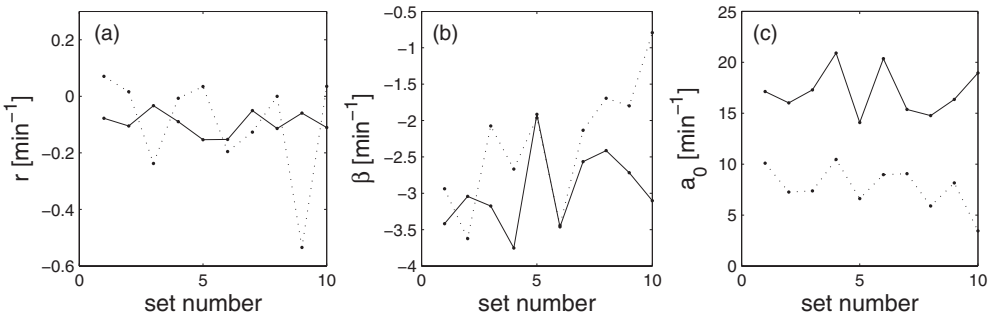

Figure 5. Values of the EU1 parameters for tumoral tissues (solid lines) and healthy tissues (dotted lines) versus the order number of the datasets.

Table 2. Values of the EU1 parameters and of the SI maximum M, as obtained by fitting the 20 DCE curves analyzed.

Parameter	Normal tissue	Tumoral tissue
r	$(0.09 \pm 0.18)\text{min}^{-1}$	$(0.09 \pm 0.04)\text{min}^{-1}$
β	$(-2.3 \pm 0.9)\text{min}^{-1}$	$(-2.9 \pm 0.5)\text{min}^{-1}$
a_0	$(7.7 \pm 2.1)\text{min}^{-1}$	$(16.8 \pm 2.8)\text{min}^{-1}$
M	(41 ± 26) au	(274 ± 89) au

tissues) in the ranges of values of both a_0 and M. Indeed, this result, i.e. the possibility of discriminating healthy from tumoral tissues by evaluating a single parameter (a_0 or M), may be very relevant from a diagnostic point of view. It is also not surprising, since tumoral tissues are more vascularized, and therefore they are characterized by a more rapid CAs uptake.

The above considerations are confirmed by figure 5, in which the values of the EU1 parameters are plotted versus the order number of the sets of data corresponding to the ten patients. In fact figures 5(a) and (b) show that the values of r and β are similar for the two cases (normal and tumoral), but more scattered for healthy tissues (dotted lines), while figure 5(c) exhibits two well-defined bands separating the ranges of values of a_0.

Finally we have also analyzed the correlation between the EU1 parameters a_0 and β. We have found that for the tumoral tissues there is a linear relationship between the two parameters

$$\beta = pa_0 \tag{12}$$

where $p = -0.175 \pm 0.030$ (see figure 6). The existence of a relative maximum M for the function $y(t)$ implies that at a certain time t_M,

$$\left[\frac{\partial y(t)}{\partial t}\right]_{t_M} = 0. \tag{13}$$

It follows

$$t_M = \frac{1}{\beta} \ln \frac{r}{r - a_0}, \tag{14}$$

and

$$M = y(t_M) = \mathrm{e}^{-1/p} \left(1 - \frac{a_0}{r}\right)^{-r/\beta}. \tag{15}$$

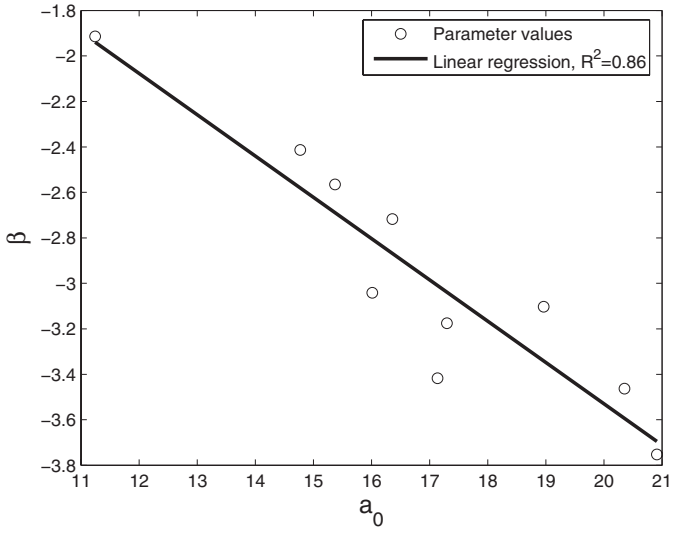

Figure 6. Linear correlation between the EU1 parameters a_0 and β for the tumoral tissues. The linear regression equation is given by equation (12).

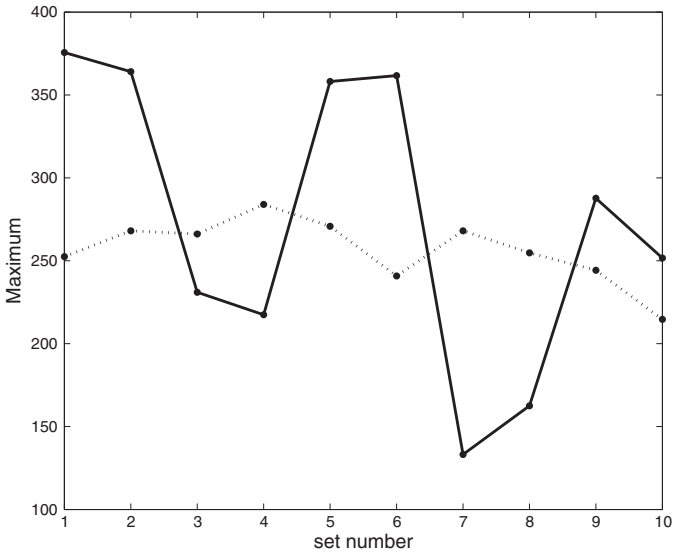

Figure 7. Maximum of the SI versus set number for tumoral tissues: experimental values (solid line: $M = 274 \pm 89$) and theoretical values as given by equation (15) (dotted line: $M = 256 \pm 20$). The value of t_M is (1.83 ± 0.31) min; see equation (14).

Using the numerical values of the parameters, as reported in table 2, the values of t_M and M can be calculated and compared with the corresponding experimental values (for tumoral tissues only); see figure 7. Since $rt_M \ll 1/p$, from equations (12) and (15), it follows that the predicted value of M is relatively constant ($M = \exp(-1/p) = 256 \pm 20$), in good agreement with the experimental results.

Discussion and conclusions

Phenomenological universalities (PUN) represent a novel tool for both cross-disciplinary and experimental research. For what concerns the first aspect, we note that the PUN approach offers a simple and systematic method for the classification of different phenomenologies, independently of their field of application. From the point of view of the interpretation of experimental datasets, PUN may be applied in many cases to find a good fitting and, when R^2 becomes close to 1, to build up a model. Since the analysis may be performed to a very high level of accuracy, it can act as a 'magnifying glass' to detect and quantify small differences among similar data.

Up to now, only one set of PUN classes had been studied in detail and applied to a variety of interdisciplinary problems, i.e. UN (Castorina *et al* 2006, Delsanto 2007, Delsanto *et al* 2009, 2008, Gliozzi *et al* 2009). In this contribution we have shown that another PUN class, i.e. EUN (see equations (9) and (10)), is well suited to solve a very important problem in the medical field, i.e. the evaluation of DCE-MRI studies. In a typical dynamic contrast enhancement (DCE) magnetic resonance imaging (MRI) session, a region of interest is selected for study and MR images are collected before, during and after a contrast agent (CA) is injected into a vein of a patient.

The power of the proposed approach lies in the capability of describing the whole process arising from the vascularization of a suspected region, using few parameters (whose interpretation is quite simple) and without making any assumption on the tissue physiology. The results of the EU1 analysis can thus be very useful in the diagnosis of a pathology. Tumors are capable of inducing blood vessel growth to supply the required nutrients, allowing for tumor expansion. The higher the lesion aggressiveness, the faster the tumor growth, depending also on tissue vascularization. In fact tumors show both an altered perfusion (which contributes to a higher vessel concentration near the lesion) and an altered permeability (which allows a better transmission of nutrients from the blood to the lesion itself). Thus the blood (with the CAs) reaches the tumor in a shorter time and in a higher amount than in normal tissues. The resulting SI and time to peak value are indicators of the altered vessel characteristics.

In a given anatomical region the maximum CA uptake of a lesion is approximately fixed, due to the presence of a 'resistance', given by surrounding structures. Also, the time to peak has a lower bound, due to bounds in the dimension of blood vessels, which limit the transport velocity of the CA. For tumors a link between the maximum SI and the time to peak (or equivalently between the EU1 parameters a_0 and β) can be established as a characteristic value for the studied lesion in a given anatomical region. Thus the values of M and t_M or p (the ratio between β and a_0) will change according to the pathology, but also with the anatomical region.

Using the normalized SI in selected ROIs has the advantage of a simple implementation since it does not need conversion to contrast concentration. Indeed the radiologist is often more interested in looking at the entire time course of contrast uptake and ROI percentage of enhancement, rather than at the numerical value of the concentration uptake. The latter requires monitoring tissue T1 before and after administration of the CA, resulting in a more time consuming examination. The EU1 parameters are linked to the initial slope of the curve, time to reach the maximum, and slope of the late phases. Thus the model is capable to describe the whole contrast wash-in and wash-out for the ROIs.

To conclude, this first study had the two goals of proposing a new method to fit DCE curves and finding applications for the universality class EUN. The results obtained on a small group of patients show that the EU1 approach is very promising. In fact it gives a better

fitting, compared with other empirical functions, e.g. the Weibull and biexponential functions (equations (1) and (2)).

A future task will be the application of the EU1 class to a large number of patients with different pathologies, in order to find out the range of values for the parameters, and also, possibly, to define threshold values to differentiate tumoral regions from non-malignant ones. It will also be interesting to study how the parameters vary for different tissues, and to compare the relative performances of EU1 and of pharmacokinetic models.

Another development will be the implementation of a pixelwise elaboration in the selected ROIs. In this study we performed a mean of the pixel SIs to test if the EU1 approach would yield useful information about the tissues under investigation. In a future work a pixel-by-pixel investigation will be performed to characterize and better define the lesions. In fact, often a tumor has a core which is different from its periphery, but a detailed analysis can be performed only if each single pixel is treated separately from the others. Fitting data from a single pixel may introduce noise error; thus, a sort of quality control on the experimental curves is necessary for a correct parameter evaluation and overall analysis.

Acknowledgment

One of the authors (AG) wishes to acknowledge the support of Regione Piemonte for his post-doc fellowship.

References

Barberis L M, Condat C A, Gliozzi A S and Delsanto P P 2010 Concurrent growth of phenotypic features: a phenomenological universalities approach *J. Theor. Biol.* **264** 123–9

Brix G, Semmler W, Port R, Schad L, Layer G and Lorenz W 1991 Pharmacokinetic parameters in CNS Gd-dTPA enhanced MR Imaging *J. Comput. Assist. Tomogr.* **15** 621–8

Buadu LD *et al* 1996 Breast lesions: correlation of contrast medium enhancement patterns on MR images with histopathologic findings and tumor angiogenesis *Radiology* **200** 639–49

Cara van P E, Ellison J J, McMurry T J and Lauffer R B 1999 Gadolinium(III) chelates as MRI contrast agents: structure, dynamics and applications *Chem. Rev.* **99** 2293–352

Castorina P, Delsanto P P and Guiot C 2006 Classification scheme for phenomenological universalities in growth problems in physics and other sciences *Phys. Rev. Lett.* **96** 188701

Claude C-J, Arslan A and Bekkelund S I 2000 MRI of the spine and spinal cord: imaging techniques, normal anatomy, artifacts, and pitfalls *J. Manipulative Physiol. Ther.* **23** 470–5

Daldrup H E, Shames D M, Husseini W, Wendland M, Okuhata Y and Brasch R 1998 Quantification of the extraction fraction for gadopentetate across breast cancer capillaries *Magn. Reson. Med.* **40** 537–43

Delsanto P P (ed) 2007 *Universality of Nonclassical Nonlinearity with applications to NDE and Ultrasonics* (New York: Springer)

Delsanto P P, Gliozzi A S, Bruno C L E, Pugno N and Carpinteri A 2009 Scaling laws and fractality in the framework of a phenomenological approach *Chaos Solitons Fractals* **41** 2782–6

Delsanto P P, Guiot C and Gliozzi A S 2008 Scaling, growth and cyclicity in biology: a new computational approach *Theor. Biol. Med. Modelling* **5** 5

Fan X, Medved M, Karczmar G S, Yang C, Foxley S, Arkani S, Recant W, Zamora M A, Abe H and Newstead G M 2007 Diagnosis of suspicious breast lesions using an empirical mathematical model for dynamic contrast-enhanced MRI *Magn. Reson. Imaging* **25** 593–603

Fayed N, Olmos S, Morales H and Modrego P J 2006 Physical basis of magnetic resonance spectroscopy and its application to central nervous system diseases *Am. J. Appl. Sci.* **3** 1836–45

Furman-Haran E and Degani H 2002 Parametric analysis of breast MRI *J. Comput. Assist. Tomogr.* **26** 376–86

Gal Y, Mehnert A, Bradley A, McMahon K and Crozier S 2007a An evaluation of four parametric models of contrast enhancement for dynamic magnetic resonance imaging of the breast *Proc. of the 29th Annu. Int. Conf. of the IEEE EMBS Cité Internationale (Lyon, France, 23–26 August)*

Gal Y, Mehnert A, Bradley A, McMahon K and Crozier S 2007b An evaluation of four parametric models of contrast enhancement for dynamic magnetic resonance imaging of the breast *IEEE Conf. on Eng. in Medicine and Biol. Society (EMBC)* pp 71–4

Gliozzi A S, Guiot C, Chignola R and Delsanto P P 2010 A phenomenological model of the oscillatory growth behavior of multicellular tumor spheroids *Cell Prolif.* **43** 344–53

Gliozzi A S, Guiot C and Delsanto P P 2009 A new computational tool for the phenomenological analysis of multipassage tumor growth curves *PLoS One* **4** e5358

Gompertz B 1825 On the nature of the function expressive of the law of human mortality and on a new mode of determining life contingencies *Phil. Trans. R. Soc. London* **123** 513

Hayton P, Brady M, Tarassenko L and Moore N 1996 Analysis of dynamic MR breast images using enhancement *Med. Image Anal.* **1** 207–24

Knopp M V, Giesel F L, Marcos H, von Tengg-Kobligk H and Choyke P 2001 Dynamic contrast-enhanced magnetic resonance imaging in oncology *Top. Magn. Reson. Imaging* **12** 301–308

Kuhl C K, Mielcareck P, Klaschik S, Leutner C, Wardelmann E, Gieseke J and Schild H H 1999 Dynamic breast MR imaging: are signal intensity time course data useful for differential diagnosis of enhancing lesions? *Radiology* **211** 101–10

Montemurro F, Russo F, Martincich L, Cirillo S, Gatti M, Aglietta M and Regge D 2004 Dynamic contrast enhanced magnetic resonance imaging in monitoring bone metastases in breast cancer patients receiving bisphosphonates and endocrine therapy *Acta Radiol.* **45** 71–74

Pickles M D, Manton D J, Lowry M and Turnbull L W 2009 Prognostic value of pre-treatment DCE-MRI parameters in predicting disease free and overall survival for breast cancer patients undergoing neoadjuvant chemotherapy *Eur. J. Radiol.* **71** 498–505

Port R E, Knopp M V, Hoffmann U, Milker-Zabel S and Brix G 1999 Multicompartment analysis of gadolinium chelate kinetics: blood-tissue exchange in mammary tumors as monitored by dynamic MR imaging *J. Magn. Reson. Imaging* **10** 233–41

Pugno N, Bosia F, Gliozzi A S, Delsanto P P and Carpinteri A 2008 Phenomenological approach to mechanical damage growth analysis *Phys. Rev.* E **78** 046013

Reddick Wilburn E, Taylor June S and Fletcher Barry D 1999 Dynamic MR imaging (DEMRI) of microcirculation in bone sarcoma *J. Magn. Reson. Imaging* **10** 277–85

Rijpkema M, Kaanders J, Joosten F, Kogel A van der and Heerschap A 2001 Method for quantitative mapping of dynamic MRI contrast agent uptake in human tumors *J. Magn. Reson. Imaging* **14** 457–63

Scalerandi M and Sansone B C 2002 Inhibition of vascularization in tumor growth *Phys. Rev. Lett.* **89** 218101

Srikanchana R, Thomasson D, Choyke P and Dwyer A 2004 A comparison of pharmacokinetic models of dynamic contrast enhanced MRI *Proc. 17th IEEE Symp. on Computer-Based Medical Systems (CBMS 2004) (Bethesda, MD, USA, 24–25 June 2004)* pp 361–6

Taber K H, Herrick R C, Weathers S W, Kumar A J, Schomer D F and Hayman L A 1998 Pitfalls and artifacts encountered in clinical MR imaging of the spine *Radiographics* **18** 1499–521

Tofts P S, Berkowitz B and Schnall M D 1995 Quantitative-analysis of dynamic Gd-dTPA enhancement in breast-tumors using a permeability model *Magn. Reson. Med.* **33** 564–8

Tofts P S and Kermode A G 1991 Measurement of blood-brain barrier permeability and leakage space using dynamic MR imaging: 1. Fundamental concepts *Magn. Reson. Med.* **17** 357–67

Tofts P S *et al* 1999 Estimating kinetic parameters from dynamic contrast-enhanced T1-weight MRI of a diffusable tracer: standardized quantities and symbols *J. Magn. Reson. Imaging* **10** 223–32

Tsekos N V, Christoforou E and Ozcan A 2008 A general-purpose MR-compatible robotic system *IEEE Eng. Med. Biol.* **27** 51–8

Tuncbilek N, Karakas H M and Altaner S 2004 Dynamic MRI in indirect estimation of microvessel density, histologic grade, and prognosis in colorectal adenocarcinomas *Abdom. Imaging* **29** 166–72

Tuncbilek N, Karakas H M and Okten O O 2005 Dynamic contrast enhanced MRI in the differential diagnosis of soft tissue tumors *Eur. J. Radiol.* **53** 500–5

Tuncbilek N, Unlu E, Karakas H M, Cakir B and Ozyilmaz F 2003 Evaluation of tumor angiogenesis with contrast-enhanced MR mammography *Breast* J **9** 403–8

van der Woude H J, Verstraete K L, Hogendoorn P C, Taminiau A H, Hermans J and Bloem J L 1998 Musculoskeletal tumors: does fast dynamic contrast-enhanced subtraction MR imaging contribute to the characterization? *Radiology* **208** 821–8

van Rijswijk C S P, Geirnaerdt Maarje J A, Hogendoorn Pancras C W, Taminiau A H M, van Coevorden F, Zwinderman A H, Pope T L and Bloem J L 2004 Soft-tissue tumors: value of static and dynamic gadopentetate dimeglumine enhanced MR imaging in prediction of malignancy *Radiology* **233** 493–502

Verstraete K L and Lang P 2000 Bone and soft tissue tumors: the role of contrast agents for MR imaging *Eur. J. Radiol.* **34** 229–46

Verstraete K L *et al* 1994 First-pass images of musculoskeletal lesions: a new and useful diagnostic application of dynamic contrast-enhanced MRI *Magn. Reson. Imaging* **12** 687–702

West G B and Brown J H 2004 Life's universal scaling laws *Phys. Today* **9** 36–42

West G B, Brown J H and Enquist B J 2000 The fourth dimension of life: fractal geometry and allometric scaling of organisms *Science* **284** 1677–9

West G B, Brown J H and Enquist B J 2001 A general model for ontogenetic growth *Nature* **413** 628

Yankeelov T E and Gore J C 2009 Dynamic contrast enhanced magnetic resonance imaging in oncology: theory, data acquisition, analysis, and examples *Curr. Med. Imaging Rev.* **3** 91–107